Method to Enhance Directional Propagation of Circularly Polarized Antennas by Making Near-Electric Field Phase More Uniform

Muhammad U. Afzal, *Senior Member, IEEE*, Ali Lalbakhsh, *Member, IEEE* and Karu P. Esselle, *Fellow, IEEE*

***Abstract*—A new approach to significantly increase the uniformity in aperture phase distribution, through time synchronization in near-electric field, of circularly polarized (CP) antennas is presented. The method uses the phase of the CP electric field vectors, obtained through full-wave numerical simulations, and does not rely on any approximation such as ray tracing. The near-field data is post-processed to extract the relative phase difference that exist due to the unsynchronized rotations of the electric field vectors in a plane parallel to the antenna aperture. The phase delay is compensated with a thin time-synchronizing metasurface (TSM) that has a 2D array of time-delay cells. The method is demonstrated with a prototype made of two-port patch antenna, which is fed through a hybrid junction, and a TSM that is placed at one wavelength spacing above the patch. When TSM is used with patch antenna, its uniform phase area increases manyfold thus increasing far-field directivity from 6.8 dBic to 22 dBic.**

***Index Terms*—Aperture field, non-uniform metasurface, patch antennas, phase distribution, phase uniformity, synchronized electric field, time synchronization.**

I. Introduction

Circularly polarized (CP) radio-frequency (RF) front-end antennas are preferred for wireless communication systems to minimize losses due to polarization mismatch when at least one of the two communicating terminals is not stationary [1]–[4]. For long-distance communication such as satellite connectivity, additionally, high-gain antennas with extremely focused energy beams are required to cater for free-space losses [5]–[10]. The gain of an antenna is directly proportional to the effective radiating aperture, which is an equivalent area that radiates a plane wave [11]. Traditionally, the effective aperture size is enhanced by arraying a large number of low-gain antennas such as microstrip patch antennas [12], [13]. One of the practical challenges associated with arrays is the additional losses of the feed network used to distribute energy from the source to individual antenna elements [14], [15]. Another commonly used practice to increase gain is to transform the phase distribution of low- to medium-gain antennas with an aim to improve phase uniformity. The latter is of great interest because it alleviates challenges associated with the feed network.

The phase transformation strategy has been used in the past to design phase-correcting lenses, transmit and reflect arrays [5], [6], [16]–[26]. The basis of all these designs is the ray-tracing technique. In this approach, first the phase is calculated by tracing a ray from the phase center of a primary feed antenna to each point in a plane parallel to the feed. The relative phase difference introduced because of the difference in the length of rays is eliminated through lens geometry or spatially distributed phase-shifting cells. Recently, electric near-field phase-correction technique has been reported with great success [27]–[29]. In the near-field method, the total height of the system is much shorter because the gap required between a phase-correcting metasurface and the base antenna is no more than one wavelength. Nevertheless, due to this close proximity, except in very special cases, approximate methods such as ray optics cannot be used for the design; instead, phase of the actual electric-field of the antenna in the near-field region is used. The numerically probed near-field phase correction based method has only been demonstrated with linearly polarized (LP) electromagnetic (EM) field.

On the other hand, upcoming satellite applications such as space internet use circularly polarized (CP) beams of EM energy to provide broadband internet through low-earth-orbit (LEO) or medium-earth-orbit (MEO) satellite constellations [30]. This paper presents a method to improve the aperture phase distribution of CP antennas. First, the phase and magnitude of two orthogonal LP field components are obtained through numerical simulations. The data is post-processed to obtain two CP near-electric field vectors, which otherwise cannot be directly obtained from numerical simulations. A thin time synchronizing metasurface (TSM) is designed to improve the phase non-uniformity of the dominant CP field component through improved time synchronization of the field vectors. The TSM is made of only a single layer of a dielectric material. On the other hand, all previously reported near-field phase-correcting surfaces used at least two dielectric layers and a bonding prepreg [28], [29]. The TSM can thus be fabricated through primitive manufacturing set up and does not rely on sophisticated facilities needed in previously reported multilayered near-field metasurfaces. The design methodology of the TSM is based on the near-field phase transformation strategy that considers the actual phase of the near-electric field data obtained through numerical simulations. This is totally different than ray-tracing based thin lenses [17], [31]–[33] designed for CP antennas. The ray-tracing based approximation, when used for antenna applications, fails to consider non-symmetries in radiating base antennas.

Muhammad Usman Afzal and Karu Esselle are with the School of Electrical and Data Engineering, University of Technology Sydney, Sydney, NSW 2007, Australia (e-mail:muhammad.u.afzal@ieee.org; karu@ieee.org). Ali Lalbakhsh is with Macquarie University.

Color versions of one or more of the figures in this paper are available online at http://ieeexplore.ieee.org.

XXX XX, 20XX; revised January XX, 20XX.

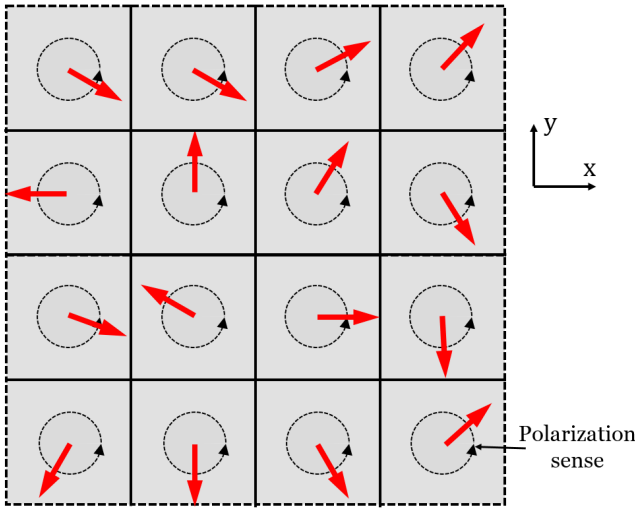

Fig. 1: A snapshot of an unsynchronized circularly polarized (CP) electric field on an hypothetical aperture. The polarization sense (field rotation) is marked with small circles whereas the electric field magnitude is indicated by the length of arrow.

The method, for the proof of concept, has been demonstrated for a simple microstrip patch antenna, which is used as the base antenna. The rest of the paper is organized such that Section II give a brief overview of the design method. A design example is discussed in Section IV and measured results are presented in Section IV of the paper.

II. Design Methodology

The design methodology of the TSM for a base antenna can be summarized in three steps. Firstly, the near-field distribution of a base antenna is obtained in a plane parallel to the antenna aperture through numerical simulations. Secondly, the phase of the co-polarized CP field component is calculated in this plane using analytical equations. Thirdly, a TSM is designed to improve the uniformity in the aperture phase distribution of the co-polar CP field component. These steps are briefly elaborated here to explain the methodology.

The base antenna is simulated using a commercial EM simulator and its near-field data is computed in an extended region around the antenna. An aperture plane is defined in a plane parallel to the base antenna and within the near-field region. The plane is divided into a finite number of 2D grid elements, as shown in Fig. 1. A fixed-time snapshot of the CP field vectors is obtained at the center of these grid points indirectly using the magnitude and phases of the Cartesian electric field components. It is known that a CP electric-field vector rotates with time, as the EM field propagates, and completes one cycle in a period 'T'. The rotating vector can be resolved into two orthogonal Cartesian field components Ex and Ey, where Ex and Ey are both complex numbers having magnitudes and phases:

$$\overrightarrow{\mathrm{E}} = |\mathrm{E_x}|\, \mathrm{e}^{\phi_\mathrm{x}}\hat{\mathrm{x}} + |\mathrm{E_y}|\, \mathrm{e}^{\phi_\mathrm{y}}\hat{\mathrm{y}}. \tag{1}$$

For CP electric field, the two Cartesian components ideally have equal magnitudes. Their phase difference $\phi_\mathrm{x} - \phi_\mathrm{y}$ is $+90^o$ and -90^o for left-hand circularly polarized (LHCP) and right-hand circularly polarized (RHCP) electric fields, respectively. The two Cartesian components are thus used to calculate the magnitude and phase of the CP electric field vectors [34]:

$$\mathrm{E_{LHCP}(x,y)} = \frac{1}{\sqrt{2}}\left(\mathrm{E_x(x,y)} - \mathrm{jE_y(x,y)}\right) \tag{2}$$

$$\mathrm{E_{RHCP}(x,y)} = \frac{1}{\sqrt{2}}\left(\mathrm{E_x(x,y)} + \mathrm{jE_y(x,y)}\right) \tag{3}$$

where $\mathrm{E_x}$ and $\mathrm{E_y}$ are complex numbers representing the magnitudes and phases of the two Cartesian field vectors.
Unsynchronized CP electric field vectors in the plane parallel to the base antenna, as depicted in Fig. 1, lead to a non-uniform aperture phase distribution. It is to be mentioned here that it is the phase of the dominant CP field component that affects the co-polar far-field directivity of the antenna. The phase (ϕ) of the dominant CP field ($\mathrm{E_{LHCP}}$ or $\mathrm{E_{RHCP}}$) is transformed into the time scale using $\mathrm{t} = \phi/\omega$ (where $\omega = \frac{2\pi}{\mathrm{T}}$ is the angular frequency) to quantify lack of synchronization within electric field in the aperture plane.
The CP field vectors are relatively time delayed in each grid cell to time synchronize the electric field in the aperture plane. For this purpose, the relative time delay is calculated in the aperture plane using:

$$\mathrm{t_d(x,y)} = \max(\mathrm{t(x,y)}) - \mathrm{t(x,y)}. \tag{4}$$

where $\mathrm{t_d(x,y)}$ is the relative time delay, $\mathrm{t(x,y)}$ is the time scale of electric on the aperture plane, and $\max(\mathrm{t(x,y)})$ is the maximum value of the aperture plane time scale. The relative time delay is introduced by inserting a 2D printed surface made of spatial time-delay cells.

III. Design Example

The proposed methodology of time-synchronizing electric field on an aperture was verified by demonstrating the working principle with a proof-of-concept design. For this demonstration, we used a microstrip patch antenna as the EM field source that was modeled and simulated with CST Microwave Studio. The patch antenna was placed in xy-plane and radiated the CP EM field at 11 GHz along +z-axis. The antenna was printed on 0.787 mm thick Rogers 5880 substrate [35] and was optimized to have a square shape with two orthogonal feeding points as shown in Fig. 2. The antenna has two quarter-wave transformers to convert impedance at the edge to $50\ \Omega$.
An external hybrid junction was used to introduce a temporal phase difference of 90^o between the two feeding ports. A hypothetical plane with a physical area of 162 mm$\times 162$ mm (or $A = X \times Y$) was considered at a spacing of one free-space wavelength (or $S = \lambda_0$) from the patch antenna. The hypothetical plane is pictorially depicted in Fig. 2(b). It is worth emphasizing here that the TSM designed to time synchronize the electric field will also be placed in this hypothetical plane. The magnitude and phase of the two Cartesian field components: $\mathrm{E_x}$ and $\mathrm{E_y}$ were probed in a 2D mesh grid in this plane, where discrete points of the grid were physically spaced by 4.26 mm (or $\sim \lambda_o/4$) along x- and y-axes. It is to be mentioned here that physical spacing between the sampling points is critical in

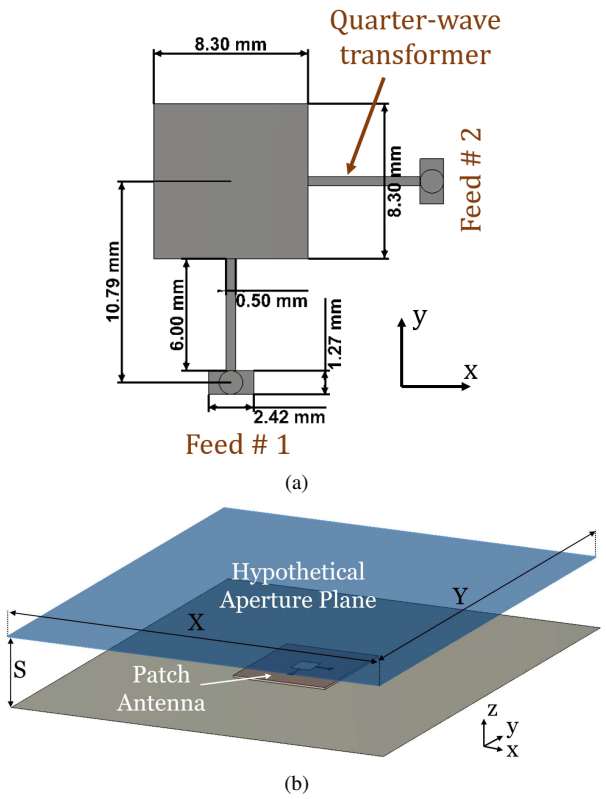

Fig. 2: (a) Top view of the microstrip patch antenna that is fed by coaxial feeds at two orthogonal ports matched to 50 ohm. (b) Perspective view of hypothetical aperture plane defined at a spacing S on top of the patch antenna.

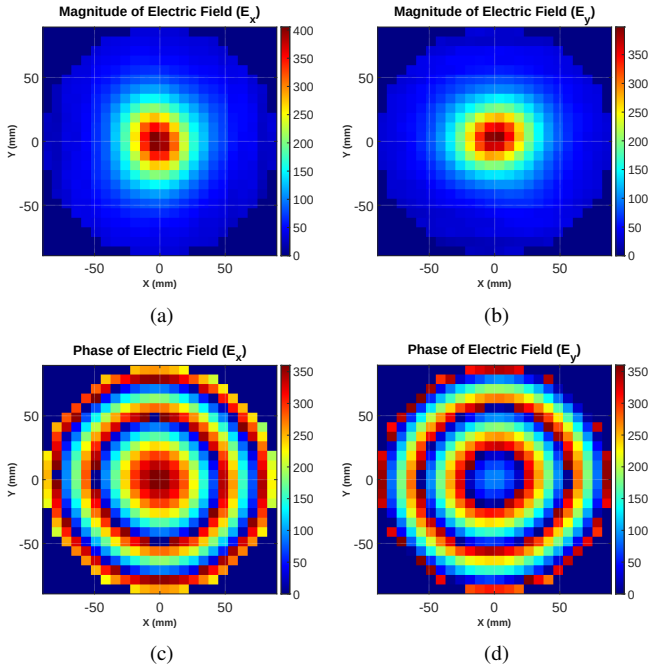

Fig. 3: Magnitude and phase of two orthogonal Cartesian field components probed at one wavelength spacing from the patch antenna ($S = \lambda_0$); (a) Magnitude of $\mathrm{E_X}$ (V/m) (b) Magnitude of $\mathrm{E_Y}$ (V/m) (c) Phase of $\mathrm{E_X}$ (d) Phase of $\mathrm{E_Y}$.

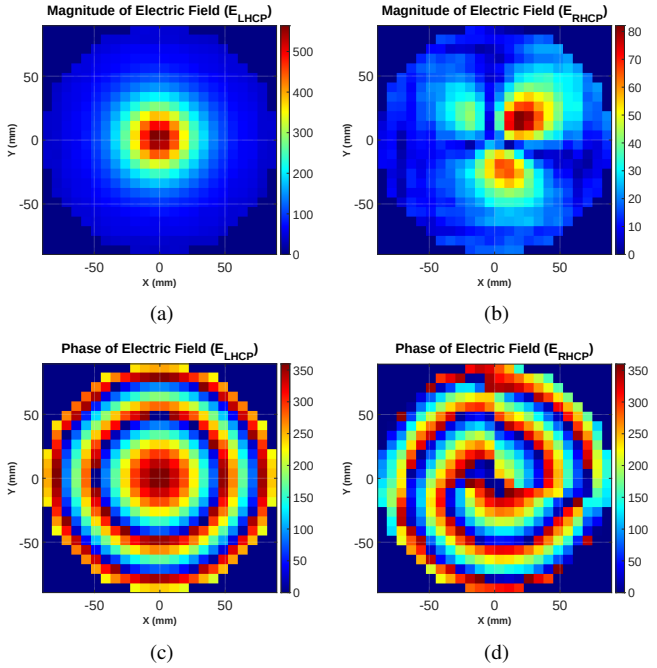

Fig. 4: Magnitude and phase of two circularly polarized field components (a) Magnitude of $\mathrm{E_{LHCP}}$ (V/m) (b) Magnitude of $\mathrm{E_{RHCP}}$ (V/m) (c) Phase of $\mathrm{E_{LHCP}}$ (d) Phase of $\mathrm{E_{RHCP}}$. Note the significant difference in vertical scales between (a) and (b).

the performance of the metasurface. A smaller step size better captures the fine variations in the aperture field distribution but is extremely difficult to implement as it requires matching sized phase-shifting cell elements. We have verified through near to far-field transformation that a sampling step of $\lambda_0/4$ was sufficient for the design.

The sampled field data is mapped on the aperture using colour combinations in Fig. 3. The data of Cartesian electric field components was used to compute the two CP field components; LHCP and RHCP with (2) and (3), respectively. The calculated amplitudes and phases of the two CP field components are mapped on the aperture in Fig. 4. The maximum amplitude of the $\mathrm{E_{LHCP}}$ is 550 V/m and the maximum amplitude of the $\mathrm{E_{RHCP}}$ is around 80 V/m. It can, therefore, be concluded that the antenna radiates LHCP field, which was expected. The phase of the LHCP was non-uniform but symmetric and that of the RHCP, which is cross-polar component, was spirally distributed.

The phase of the LHCP was first normalized so that phase values are between 0^{o} and 360^{o}, which was then transformed to a time scale between 0 and T. The time scale data was used to calculate the relative time-delay required at each sampled point in order to time synchronize the unsynchronized rotation of electric field vectors, which is visually represented on a normalized scale in Fig. 5. This time delay was implemented with a thin TSM made of cell elements similar to that used in [17]. The cell element has an identical printed pattern on both sides of a thin dielectric layer, which is discussed in the following section.

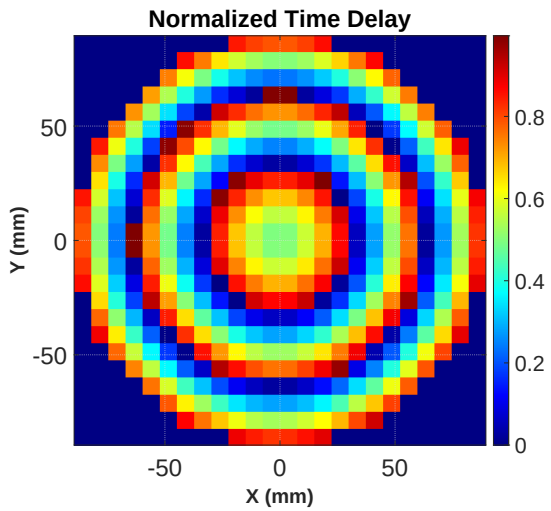

Fig. 5: Normalized time delay between 0 and T required to time synchronize the CP electric field.

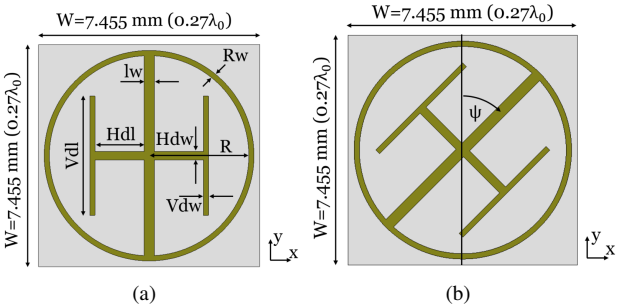

Fig. 6: Configuration of time-delay cell (a) Critical dimensions in millimetre and λ_0: Hdl=1.65 mm or $0.06\lambda_0$, Hdw=0.28 mm $0.01\lambda_0$, Vdl=4 mm or $0.15\lambda_0$, Vdw=0.175 mm or $0.06\lambda_0$, R=3.36 mm or $0.12\lambda_0$, Rw=0.175 mm or $0.06\lambda_0$, lw=0.35 mm or $0.013\lambda_0$ and (b) Physical rotation angle that controls the time delay of the cross-polar transmitted-field component. The golden stripes represent the printed pattern and the grey area is the dielectric material.

A. Time-Delay Cell Element

The type of cells used for most LP antennas and some CP antennas have a stack of alternating dielectric and metal layers [19], [36], [37]. These cells introduce a phase shift without changing the polarization of the propagating electric field. However, for CP electric field, there are other thin cell configurations that transform an incoming LHCP electric field into an RHCP transmitted electric field or vice versa [17], [32], [33]. In these types of cell elements, the time delay of the transmitted field is simply controlled by the rotation angle of the printed pattern on the cells. One such time-delay cell used here for the demonstration has a conductive printed pattern on both sides of a dielectric layer. The conductive printed pattern has a circular ring and two orthogonal metallic features.

The important dimensions of the unit cell are labeled in Fig. 6(a). The golden traces represent the printed conductive pattern and the grey area is the 1.57 mm thick Taconic TLY-5 dielectric material [38]. It is to be mentioned here that only the top layer is shown in the figure and an identical layer exists on the bottom side of the dielectric material. This unit

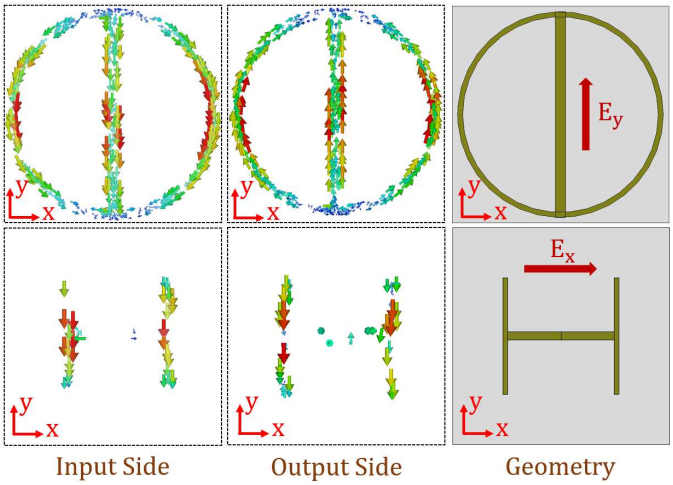

Fig. 7: The surface currents at the input and output sides of the time-delay unit cell with partial metallic features and when excited by one of the two orthogonal field components.

cell was simulated with the periodic boundary conditions in the lateral directions. The two de-embedded ports were used at the input and output along the z-axis. The horizontal and vertical metallic features in the time-delay cell resonate when excited by one of the two orthogonal field components. To investigate this further, horizontal and vertical features of the cell were separately excited with the two orthogonal field components; E_x and E_y, respectively. The circular ring and the connecting vertical section was excited with E_y and the H-shaped horizontal section was excited with Ex, as shown in Fig. 7. The vertical field component (E_y) was transmitted due to the resonance of the ring and the attached vertical metallic feature. However, as visible in the top row of the pictures in Fig. 7, the surface currents at the input and output sides of the cell are pointing in opposite directions, indicating an out-of-phase transmission (or 180^o phase shift) of the vertical component. The horizontal electric-field component (or E_x) was transmitted due to the resonance of an H-shaped metallic feature on the unit cell. It is important to note that the directions of the surface currents at the input and output sides of the unit cell are the same, indicating an in-phase transmission of the horizontal field component. The transmission magnitudes of both E_x and E_y were greater than -0.5 dB and only E_y experiences a transmission-phase shift of $\sim 180^o$. It is well known that a phase shift of 180^o in one of the Cartesian field components, relative to the other, changes the sense of the CP field, which in this case was from LHCP to RHCP. In addition, the cell introduces a phase shift or time delay, which is discussed below with more details.

The unit cell performance was further analyzed for the propagating Floquet space harmonics and an LHCP field was excited from the input port. The co- and cross-polar reflected and transmitted electric fields were observed at both input and output ports, respectively. The unit-cell dimensions were optimized such that most of the incoming LHCP field was coupled into the outgoing RHCP field. The transmitted RHCP field component experiences a time or phase delay, which is controlled by the clockwise physical rotation angle of the

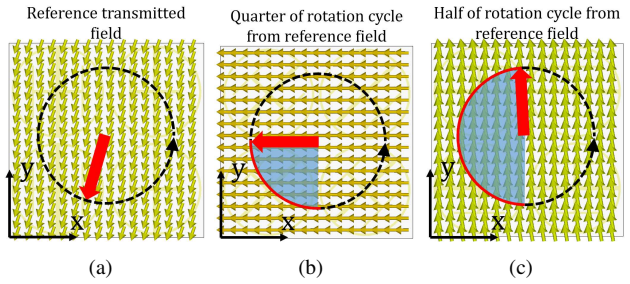

Fig. 8: Transmitted RHCP electric field at the same instant of time for three different values of ψ, the rotation sense of the electric field is displayed. (a) $\psi = 0$ and the direction of the transmitted electric field is used as a reference, for $\psi = 45$ and $\psi = 90$ the electric vectors in (b) and (c), are delayed by $\sim T/4$ and $\sim T/2$, respectively.

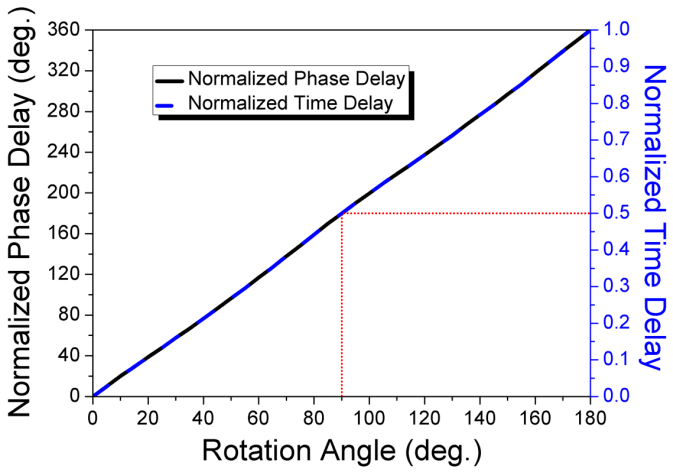

Fig. 9: Normalized phase and time delays experience by transmitted field through the unit cell with different rotation angles (ψ).

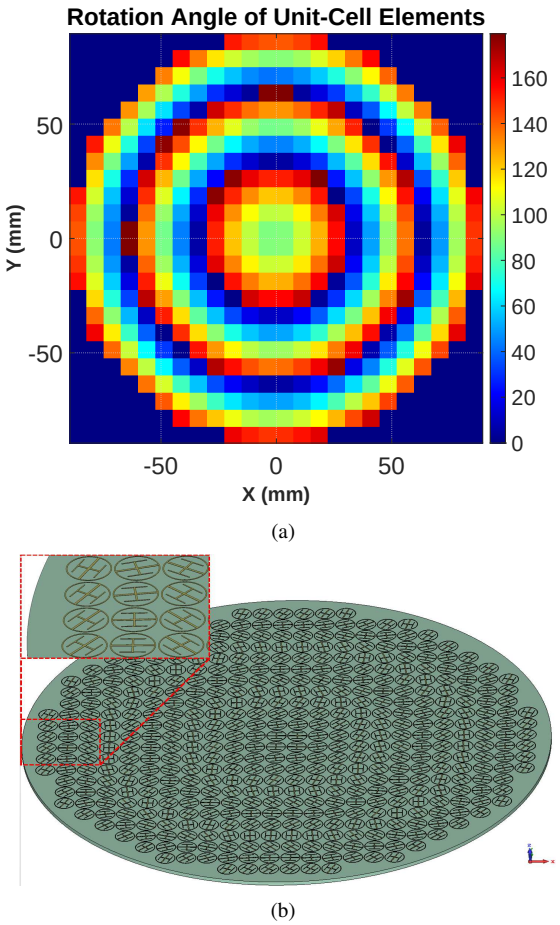

Fig. 10: (a) Rotation angles (ψ) of the unit cell mapped on the aperture. (b) A perspective view of the TSM model with a close up in the inset, an identical conductive pattern exists at the bottom of the TSM, which is not visible in the figure.

printed pattern, represented by symbol ψ in Fig. 6(b). As an example, a snapshot of the electric field vector in the transmitted region for $\psi = 0^o, 45^o$, and 90^o are shown in Fig.8. The time-delay of the cross-polar transmitted field component was normalized such that the time delay is 0 when $\psi = 0$. The time delay was calculated directly from the phase delay (or $\Delta\phi$) obtained from unit-cell simulations using $\Delta t = \Delta\phi/\omega$. The exact values of time- and phase-delay obtained from the unit cell simulations are plotted against ψ in Fig. 9.

B. Time-Synchronizing Metasurface

To build the aperture of TSM, the cell elements were appropriately rotated to provide the required time delays. To do this, the required time-delay data given in Fig. 5 was used to find cells from the time-delay plot given in Fig. 9. As an example, at the center of the aperture in Fig. 5, a normalized time delay of $\sim$0.5T was required, which according to Fig. 9 can be obtained from a unit cell that has $\psi = 90$, i.e. the printed pattern was rotated by $\sim 90^o$ angle. In this manner, the TSM aperture was populated with the corresponding cell elements. The rotation angles of cells mapped on the aperture of the TSM are shown in Fig. 10(a) and a perspective view of the resulting 3D model of the TSM is shown in Fig. 10(b).

The improvement in time synchronization with the TSM was verified by simulating it with the previously described patch antenna, in CST Microwave Studio. Furthermore, the results predicted through numerical simulations were validated by the measurements of a prototype. The prototype was measured in NSI spherical near-field measurement system. The predicted and measured results of the prototype design are discussed in the following section.

IV. Measured Results

The patch antenna with the TSM was simulated and both near- and far-field results were analyzed. The time synchronization in the radiated electric field with the TSM was quantified by analytically calculating the phase of the dominant CP electric field component above the TSM. An indirect approach was adopted and first, the phases of the two Cartesian field components were probed at a discrete number of points on the aperture of the antenna. The data was used to calculate the magnitude and phase of the two CP electric fields, i.e. RHCP and LHCP. The color plots of the amplitude and the phase of the dominant, RHCP, field component are mapped on the aperture in Fig. 11.

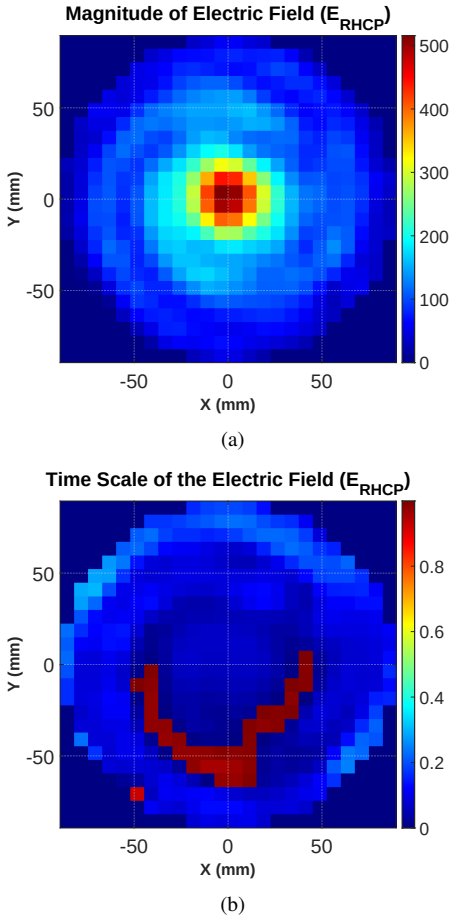

Fig. 11: Magnitude and phase of the dominant RHCP electric field mapped to the aperture above TSM. The field is concentrated in the center of the aperture while the phase is nearly uniform, visible by less variation in colors.

The highest amplitude of the E_{RHCP} is $\sim$ 520 V/m at the center of the aperture. The phase of E_{RHCP} was then transformed into the time scale using angular frequency. The time synchronization in the electric field was reflected in the phase of the radiated electric field. The positive influence in the time synchronization of the electric field was also reflected in the far-field directivity patterns of the antenna in the direction normal or broadside to the antenna aperture. The far-field radiation patterns were observed in a frequency band around the central operating frequency of 11 GHz. The elevation pattern cuts were taken at two azimuth angels: $\phi = 0^o$ and $\phi = 90^o$. Normalized patterns cuts are given in Fig. 14. The predicted peak directivity of the patch antenna with the TSM was around 22 dBic in the broadside, which was about 15 dB more than that of the patch antenna without TSM in the same direction.

The front side of the built prototype is on the left in Fig. 12, while the backside with a hybrid junction and the RF cables is on the right of the figure. The hybrid junction was used to obtain the temporal phase difference of 90^o between the two input ports of the patch antenna. The input ports of the antenna have reasonable impedance matching around the central operating frequency, as shown in Fig. 13. As a reference, the variation in

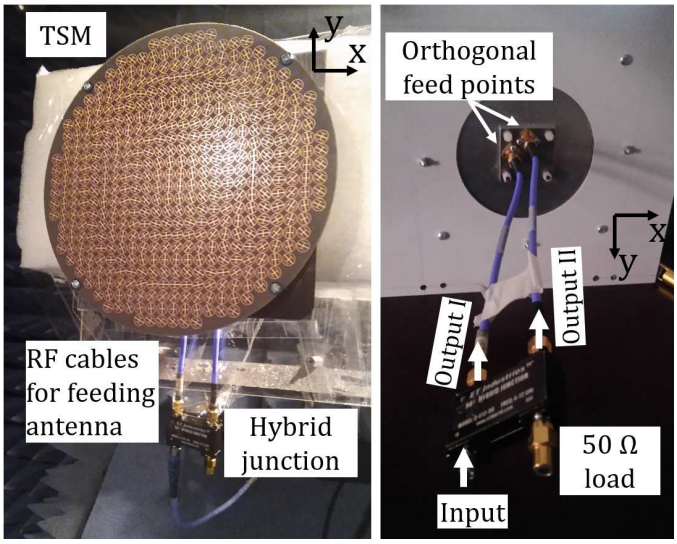

Fig. 12: Photographs of the fabricated prototype: (left) front view showing metasurface and Hybrid junction and (right) back view showing two orthogonal feeding points of the microstrip patch antenna.

reflection magnitude with the TSM is also given in the figure. It is evident from the results that the loading of the antenna by the TSM does not have a significant impact on the impedance matching. This is because: (a) The TSM was designed using unit cells that have very high transmission magnitude and (b) The TSM was placed at a spacing of one wavelength from the patch antenna. In prototyping, plastic spacers were used to suspend the TSM over the patch antenna.

The far-field patterns were measured in a frequency band between 10.5 GHz to 11.5 GHz with a step of 0.1 GHz. In the broadside, along +z-axis, the maximum directivity of 22 dBic was achieved at 11 GHz. It is worth emphasizing here that the directivity of the patch antenna without TSM in the same direction was only 6.8 dBic. The far-field pattern cuts, with the TSM, taken at two azimuth angles $\phi = 0$ and $\phi = 90$ are given in Fig. 14(a) and Fig. 14(b), respectively. The high sidelobe levels in measured patterns, particularly at azimuth angle ($\phi = 0^o$), are attributed to the diffractions from the edges of the extended ground plane and scattering from the support structure used to fix the antenna in the anechoic chamber. The antenna has acceptable cross-polar rejection with cross-polar components at least 20 dB less than the co-polar component in the main beam direction. The polarization purity or the cross-polar rejection can be increased further using a feed antenna with lower cross-polar components. Similarly, the time-delay element of the TSM can also be optimized to reject the overall cross-polar component of the antenna system.

The measured broadside gain at the operating frequency of 11 GHz is 19.8 dBic and was about 2 dB less than the measured directivity. The 2 dB loss was contributed by the RF cables and the hybrid coupler used in the feeding arrangement of the patch antenna. To investigate this further, we have characterized both RF cables and the hybrid junction using a network analyzer. The magnitude of the transmission coefficient for these components is plotted in Fig. 15. At the operating frequency, the insertion loss of each cable was around 0.4 dB, thus contributing a total

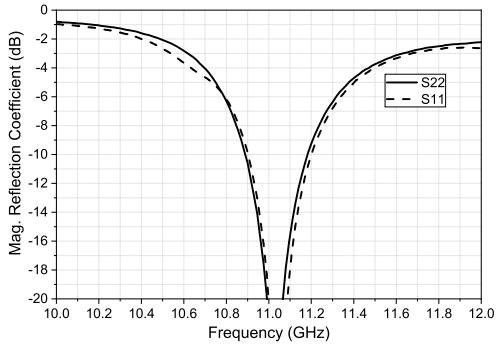

(a)

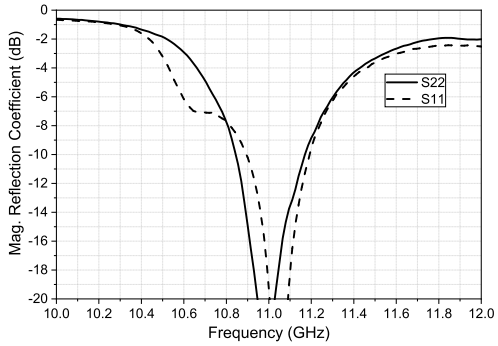

(b)

Fig. 13: Magnitude of the reflection coefficient measured at the two orthogonal input ports of the microstrip patch antenna. (a) Without metasurface and (b) With metasurface.

loss of 0.8 dB. The insertion loss measured at 0^o and 90^o phase ports of the hybrid junction was 0.2 dB and 0.7 dB, respectively. The total insertion loss at the operating frequency was around 1.8 dB. The axial ratio in the direction of beam peak was less than 3 dB, which is evident by the axial ratio pattern cuts taken at the two azimuth angles, given in Fig. 16. The peak gain and directivity variation within a finite frequency band around the operating frequency is shown in Fig. 17. It can be seen that gain is closer to directivity at the frequency points where the antenna has matched impedance. Despite being a narrow band structure, the 3 dB directivity and gain bandwidth are at least 600 MHz, which is sufficient for receiving Ku-band satellite services. One of the important factors that determine the overall bandwidth of the phase-correcting metasurface based antennas is the transmission bandwidth of the cell, which is the building block of the metasurface. To investigate the performance of the cell used here, the magnitude of the transmitted field component is plotted in Fig. 18. The -1dB transmission bandwidth is between 10.8 GHz to 11.3 GHz and the -3dB transmission bandwidth is in the frequency band between 10.6 GHz to 11.6 GHz. At a frequency where the transmission magnitude of the cell is low, the metasurface behaves as a reflector rather than a transmitting surface, which violates the fundamental requirement of a phase-correcting metasurface or a TSM. The unique aspect of the proposed time-synchronization strategy is that it uses the phase of actual CP electric-field vectors, unlike the approximated ray-tracing method that does not cater to the

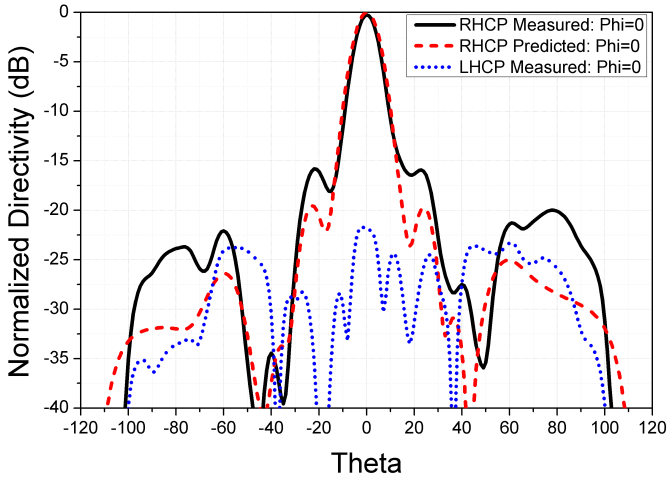

(a)

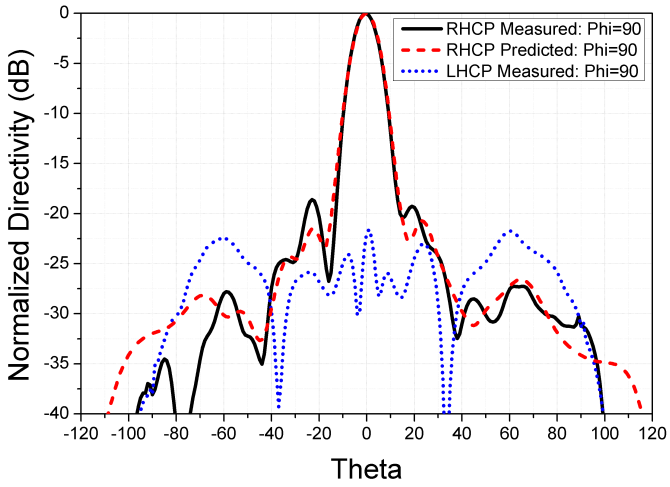

(b)

Fig. 14: Comparison of predicted and measured normalized far-field pattern cuts taken at azimuth angles: (a) $\phi = 0^o$ and (b) $\phi = 90^o$. The cross-polar components in both planes are also included for reference.

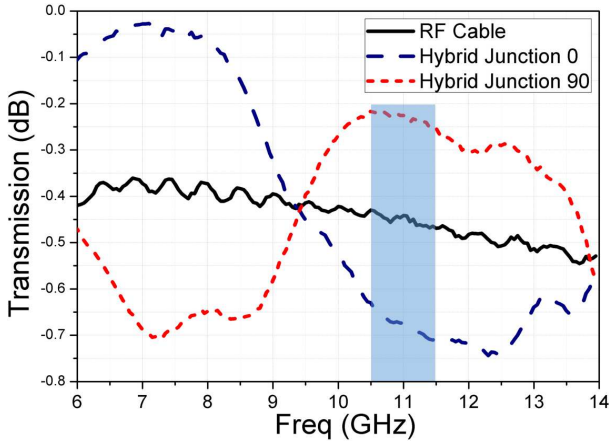

Fig. 15: Transmission through RF cables and the hybrid junction used to feed the patch antenna.

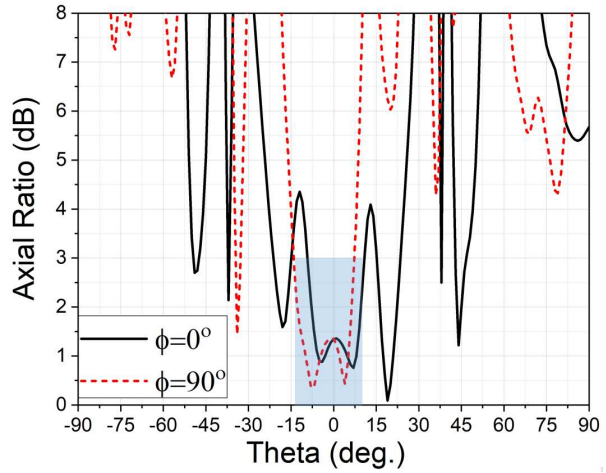

Fig. 16: Axial ratio at the operating frequency taken at two azimuth angles: $\phi = 0^{\circ}$ and $\phi = 90^{\circ}$.

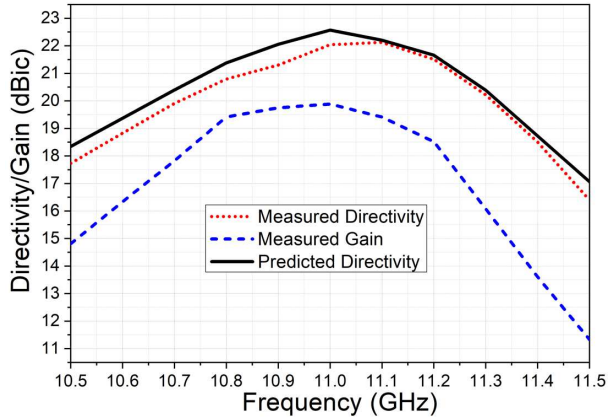

Fig. 17: Broadside directivity and gain variation with frequency. Peak directivity predicted from full-wave simulations is included for comparison.

physical asymmetry of the base antenna. The method does not have any fundamental limitation and can easily be extended to large apertures high-gain antennas such as radial-line slot arrays [10], [39], metasurface antennas [40], and even antenna arrays.

V. Conclusion

A new method to increase significantly the directivity of a simple circularly polarized (CP) antenna through improved time-synchronization of the electric field vectors on a plane in the near-field region is presented. The proof-of-concept design uses a patch antenna that is fed at two orthogonal input points through a hybrid junction for introducing a temporal phase difference of 90°. The time-synchronization is achieved in an extended plane parallel to the antenna aperture using a time-synchronizing metasurface (TSM). The TSM comprises spatially distributed time-delay cells to appropriately delay the rotation of CP electric field vectors. Through improved time-synchronization, the far-field directivity of the patch antenna is increased from 6.8 dBic to 22 dBic and the 3dB beamwidth is reduced from 114° to 11.1°. Unlike ray-tracing based lenses,

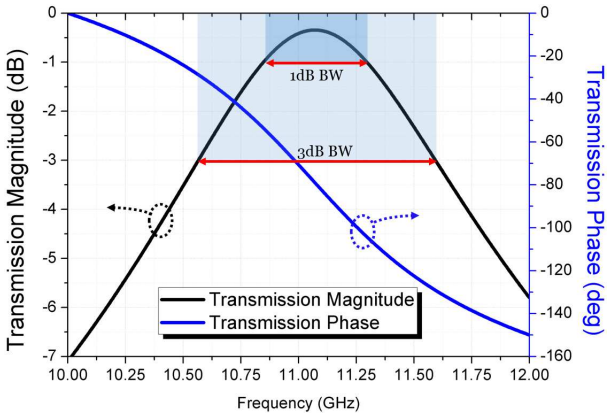

Fig. 18: Transmission phase and magnitude of the time-delay unit cell in a frequency band around the operating frequency.

the proposed design method uses data of the actual near field, which in this case was computed using detailed full-wave numerical simulations.

Acknowledgement

We acknowledge the support of Australian Research Council (ARC) Discovery grant and a strategic start-up grant provided by Faculty of Engineering and IT, University of Technology Sydney, Australia.

References

[1] G. Ganaraj, C. Kumar, and V. S. Kumar and, "High gain circularly polarized resonance cavity antenna at x-band," in *2017 IEEE International Conference on Antenna Innovations Modern Technologies for Ground, Aircraft and Satellite Applications (iAIM)*, Nov 2017, pp. 1–5.

[2] L. Gan, W. Jiang, S. Gong, Q. Chen, and X. Li, "A low-profile and high-gain circularly polarized antenna based on holographic principle," in *2018 Asia-Pacific Microwave Conference (APMC)*, Nov 2018, pp. 1031–1033.

[3] K. W. Linnes, W. D. Merrick, and R. Stevens, "Ground antenna for space communication system," *IRE Trans. on Space Electronics Telemetry*, vol. SET-6, no. 1, pp. 45–54, March 1960.

[4] H. Yang, J. An, H. Jung, J. Kim, and J. T. S. Sumantyo, "Circular polarization implementation on synthetic aperture radar," in *2014 International Conference on Information and Communication Technology Convergence (ICTC)*, Oct 2014, pp. 991–994.

[5] H.D. Hristov and M.H.AJ. Herben, "Millimeter-wave Fresnel-zone plate lens and antenna," *IEEE Trans. Microw. Theory Techn.*, vol. 43, no. 12, pp. 2779–2785, Dec 1995.

[6] Y. Ji and M. Fujita, "Design and analysis of a folded Fresnel zone plate antenna," *Int. J. Infrared Millimeter Waves*, vol. 15, no. 8, pp. 1385–1406, 1994.

[7] A. P. Feresidis and J.C. Vardaxoglou, "High gain planar antenna using optimised partially reflective surfaces," *Microw. Antennas Propag., IEE Proceedings*, vol. 148, no. 6, pp. 345–350, Dec 2001.

[8] F. E. Tubbal, R. Raad, and K. Chin, "A survey and study of planar antennas for pico-satellites," *IEEE Access*, vol. 3, pp. 2590–2612, 2015.

[9] L. H. Abderrahmane and M. Benyettou, "A ka band offset dish antenna to be used for the future algerian telecommunication satellite," in *2007 IEEE Aerospace Conference*, March 2007, pp. 1–5.

[10] M. Ando, K. Sakurai, N. Goto, K. Arimura, and Y. Ito, "A radial line slot antenna for 12 ghz satellite tv reception," *IEEE Transactions on Antennas and Propagation*, vol. 33, no. 12, pp. 1347–1353, December 1985.

[11] R. Haupt, "Generating a plane wave with a linear array of line sources," *IEEE Transactions on Antennas and Propagation*, vol. 51, no. 2, pp. 273–278, Feb 2003.

[12] L. Kouhalvandi, S. Paker, and H. B. Yagci, "Ku - band slotted rectangular patch array antenna design," in *2015 23nd Signal Processing and Communications Applications Conference (SIU)*, May 2015, pp. 447–450.

[13] X. Cai, W. Geyi, and H. Sun, "A printed dipole array with high gain and endfire radiation," *IEEE Antennas and Wireless Propagation Letters*, vol. 16, pp. 1512–1515, 2017.
[14] C. Li, Y. Wang, and Z. Zhang, "A feed network of microstrip array antenna," in *2017 IEEE 2nd Information Technology, Networking, Electronic and Automation Control Conference (ITNEC)*, Dec 2017, pp. 1764–1767.
[15] J. Thakur, M. Tamang, and K. P. Ray, "X-band hybrid feed network for antenna," in *2019 6th International Conference on Signal Processing and Integrated Networks (SPIN)*, March 2019, pp. 698–703.
[16] Y. Zhang, R. Mittra, and W. Hong, "Systematic design of planar lenses using artificial dielectrics," in *IEEE AP-S Int. Symp.*, 2010, pp. 1–4.
[17] Di Zhang, Xiaoqing Yang, Piqiang Su, Jiefang Luo, Huijie Chen, Jianping Yuan, and Lixin Li, "Design of single-layer high-efficiency transmitting phase-gradient metasurface and high gain antenna," *Journal of Physics D: Applied Physics*, vol. 50, no. 49, pp. 495104, nov 2017.
[18] N. Gagnon, A. Petosa, and D.A. McNamara, "Printed hybrid lens antenna," *IEEE Trans. Antennas Propagat.*, vol. 60, no. 5, pp. 2514–2518, 2012.
[19] M. A. Al-Joumayly and N. Behdad, "Wideband planar microwave lenses using sub-wavelength spatial phase shifters," *IEEE Trans. Antennas Propagat.*, vol. 59, no. 12, pp. 4542–4552, Dec 2011.
[20] He Wang, Yongfeng Li, Yajuan Han, Sai Sui, and Jiafu Wang, "A circular-polarized metasurface planar reflector antenna based on pancharatnam–berry phase," *Applied Physics A*, vol. 125, 03 2019.
[21] Z. Li, J. Su, and Z. Li, "A novel high-gain circularly polarized planar lens antenna based on the element rotation method," in *2017 Sixth Asia-Pacific Conference on Antennas and Propagation (APCAP)*, Oct 2017, pp. 1–3.
[22] He Wang, Yongfeng Li, Yajuan Han, Ya Fan, Sai Sui, Hongya Chen, Jiafu Wang, Qiang Cheng, Tiejun Cui, and Shaobo Qu, "Vortex beam generated by circular-polarized metasurface reflector antenna," *Journal of Physics D: Applied Physics*, vol. 52, no. 25, pp. 255306, apr 2019.
[23] Z. H. Jiang and X. Zhu, "An integrated, broadband circularly-polarized millimeter-wave metasurface-based transmit-array," in *2019 International Applied Computational Electromagnetics Society Symposium (ACES)*, April 2019, pp. 1–2.
[24] Haipeng Li, GuangMing Wang, Tong Cai, JianGang Liang, and Haisheng Hou, "Bifunctional circularly-polarized lenses with simultaneous geometrical and propagating phase control metasurfaces," *Journal of Physics D: Applied Physics*, vol. 52, no. 46, pp. 465105, sep 2019.
[25] Haisheng Hou, Haipeng Li, Guangming Wang, Tong Cai, Xiangjun Gao, and Wenlong Guo, *High Performance Metasurface Antennas*, 08 2019.
[26] X. Meng, J. Wu, Z. Wu, T. Qu, and L. Yang, "Design of multiple-polarization reflectarray for orbital angular momentum wave in radio frequency," *IEEE Antennas and Wireless Propagation Letters*, vol. 17, no. 12, pp. 2269–2273, Dec 2018.
[27] M. Afzal, K. Esselle, and B. Zeb, "Dielectric phase correcting structures for electromagnetic band gap resonator antennas," *IEEE Trans. Antennas propagat.*, vol. PP, no. 99, pp. 1–1, 2015.
[28] M.U. Afzal and K.P. Esselle, "A low-profile printed planar phase correcting surface to improve directive radiation characteristics of electromagnetic band gap resonator antennas," *Antennas and Propagation, IEEE Transactions on*, vol. 64, no. 1, pp. 276–280, Jan 2016.
[29] A. Lalbakhsh, M. U. Afzal, and K. P. Esselle, "Multiobjective particle swarm optimization to design a time-delay equalizer metasurface for an electromagnetic band-gap resonator antenna," *IEEE Antennas and Wireless Propagation Letters*, vol. 16, pp. 912–915, 2017.
[30] V. Rojansky and M. Winebrand, "Development of broadband circular polarized planar antenna for "eros" leo satellite," in *IEEE Antennas and Propagation Society International Symposium. 2001 Digest. Held in conjunction with: USNC/URSI National Radio Science Meeting (Cat. No.01CH37229)*, July 2001, vol. 2, pp. 30–33 vol.2.
[31] K. Liu, G. Wang, W. Guo, and H. Hou, "Design of high efficiency single-layered transparent metasurface and its application for circularly polarized lens antenna," in *2018 IEEE MTT-S International Wireless Symposium (IWS)*, May 2018, pp. 1–4.
[32] T. Li and J. Liang, "Single-layer transparent focusing metasurface and its application to high gain circularly polarized lens antenna," in *2016 IEEE International Workshop on Electromagnetics: Applications and Student Innovation Competition (iWEM)*, May 2016, pp. 1–3.
[33] Z. Li, J. Su, and Z. Li, "Realization of high-gain circularly polarized planar lens antenna with beam steering capability," in *2018 International Applied Computational Electromagnetics Society Symposium - China (ACES)*, July 2018, pp. 1–2.
[34] B. Y. Toh, R. Cahill, and V. F. Fusco, "Understanding and measuring circular polarization," *IEEE Transactions on Education*, vol. 46, no. 3, pp. 313–318, Aug 2003.
[35] Rogers, "RT duroid 5880 laminates," Available:https://rogerscorp.com/en/advanced-connectivity-solutions/rt-duroid-laminates/rt-duroid-5880-laminates.
[36] H. Kaouach, "Design and characterization of circularly polarized discrete lens antennas in 60-ghz band," *IEEE Antennas and Wireless Propagation Letters*, vol. 15, pp. 1200–1203, 2016.
[37] C. Tian, Y. Jiao, and G. Zhao, "Circularly polarized transmitarray antenna using low-profile dual-linearly polarized elements," *IEEE Antennas and Wireless Propagation Letters*, vol. 16, pp. 465–468, 2017.
[38] Taconic, "Taononic advanced dielectric division," Available:https://www.4taconic.com/page/tly-87.html.
[39] N. Y. Koli, M. U. Afzal, K. P. Esselle, and M. Z. Islam, "Investigation on aperture field distribution of circularly polarised radial line slot array antennas," in *2018 IEEE Asia-Pacific Conference on Antennas and Propagation (APCAP)*, Aug 2018, pp. 462–463.
[40] G. Minatti, M. Faenzi, E. Martini, F. Caminita, P. De Vita, D. González-Ovejero, M. Sabbadini, and S. Maci, "Modulated metasurface antennas for space: Synthesis, analysis and realizations," *IEEE Transactions on Antennas and Propagation*, vol. 63, no. 4, pp. 1288–1300, April 2015.

Muhamamd Usman Afzal IEEE M' (2017), SM (2020), is a Research Fellow working at the University of Technology Sydney. Muhammad received the Bachelor in Electronics Engineering and Masters in Computational Science and Engineering from the National University of Sciences and Technology (NUST), Islamabad, in 2009 and 2011, respectively. He received PhD in Electronics Engineering from Macquarie University, Australia, in 2017. He developed the concept of near-field phase transformation during his doctorate research, which was demonstrated to enhance the directivity of low-gain aperture antennas in IEEE TAP paper entitled "Dielectric phase-correcting structures for electromagnetic band-gap resonator antennas". He is the co-inventor of efficient antenna beam-steering technology referred to as Near-Field Meta-Steering. This technology received the "Highly Commended" certificate in the Five Future-Shaping Research Priorities category in the 2017 Academic Staff Awards at Macquarie University. To commercialize the outcomes of his research, he led a team of colleagues in a CSIRO sponsored ON Prime 2 in 2017 – a pre-accelerator program designed to commercialize outcomes of academic research in Australia.

Muhammad started his professional career as a Lab Engineer in 2010 at Research Institute for Microwave & Millimetre-Wave Studies (RIMMS) NUST, Islamabad. In 2012, he was promoted to the position of lecturer, which he continued till Feb 2013. In 2017, after PhD, he was offered a post-doctorate for three years on a project funded by the Australian Research Council (ARC) through the Discovery grant scheme at Macquarie University. Apart from the project-specific research, Muhammad co-supervised one PhD, three Masters of research, and several undergraduate thesis students at Macquarie University.

He has received several awards and scholarships, including a merit-based scholarship in six out of eight semesters during the undergraduate degree, a scholarship of complete fee waiver during the postgraduate degree, and the international Macquarie Research Excellence (iMQRES) scholarship towards Doctorate study from Macquarie University. He received a competitive travel grant in 2015 to present my research work at a flagship conference under the Antennas and Propagation Society (APS) in Vancouver, Canada. He assisted in preparing several grant applications, including a successful ARC discovery grant in 2018. He was the third CI in a team of five who received a grant of more than AUD 20K from the German Academic Exchange Service in a funding scheme "Australia-Germany Joint Research Co-Operation Scheme". He is currently working on the development of satellite-terminal antenna technology and has research interests in electromagnetic phase-shifting structures, frequency selective surfaces, and similar metamaterials for microwave and millimeter-wave antenna applications.

Ali Lalbakhsh received the B.S. and M.S degrees in electronic and telecommunication engineering from Islamic Azad University, Iran, in 2008 and 2011, respectively. He received the Master of Research degree (HD) and the Ph.D. in electronics engineering from Macquarie University, Australia in 2015 and 2020, respectively, and he is currently a sessional academic in the same institution. He has authored and co-authored around 60 peer-reviewed journal and conference papers so far. His research interests include resonance-based antennas, frequency selective surfaces, electromagnetic metasurfaces, periodic and electromagnetic band gap structures, evolutionary optimisation methods, and microwave passive components. Mr. Lalbakhsh received several prestigious awards including an international Research Training Program scholarship (iRTP) for the MRes, international Macquarie University Research Excellence Scholarship (iMQRES) for the PhD, Commonwealth Scientific and Industrial Research Organization (CSIRO) grants on Astronomy and Space exploration, Macquarie University Postgraduate Research Fund (PGRF) and WiMed Travel Support Grants. He was a recipient of the 2016 ICEAA-IEEE APWC Cash Prize and Macquarie University Deputy Vice-chancellor commendation in 2017. Ali is the only researcher in IEEE Region 10 (Asia-Pacific) who has won the most prestigious Best Paper Contest of IEEE Region 10 more than once. He was awarded First, Second and Third Prices in this international competition in 2018, 2019 and 2016, respectively. He is nominated for the 2019 Excellence in Higher Degree Research Award-Science, Technology, Engineering, Mathematics and Medicine (STEMM) at Macquarie University. Ali is as an Associate Editor of AEÜ - International Journal of Electronics and Communications.

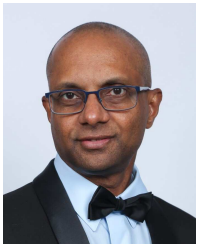

Karu Esselle IEEE M' (1992), SM (1996), F (2016) is the Distinguished Professor in Electromagnetic and Antenna Engineering at the University of Technology Sydney and a Visiting Professor of Macquarie University, Sydney. According to 2019 Special Report on Research published by The Australian national newspaper, he is the National Research Field Leader in Australia in both Microelectronics and Electromagnetisms fields.

Karu received BSc degree in electronic and telecommunication engineering with First Class Honours from the University of Moratuwa, Sri Lanka, and MASc and PhD degrees with near-perfect GPA in electrical engineering from the University of Ottawa, Canada. Previously he was Director of WiMed Research Centre and Associate Dean – Higher Degree Research (HDR) of the Division of Information and Communication Sciences and directed the Centre for Collaboration in Electromagnetic and Antenna Engineering at Macquarie University. He has also served as a member of the Dean's Advisory Council and the Division Executive and as the Head of the Department several times. Karu is a Fellow of the Royal Society of New South Wales, IEEE and Engineers Australia.

Since 2018, Karu has been chairing the prestigious Distinguished Lecturer Program Committee of the IEEE Antennas and Propagation (AP) Society – the premier global learned society dedicated for antennas and propagation - which has close to 10,000 members worldwide. After two stages in the selection process, Karu was also selected by this Society as one of two candidates in the ballot for 2019 President of the Society. Only three people from Asia or Pacific apparently have received this honour in the 68-year history of this Society. Karu is also one of the three Distinguished Lecturers (DL) selected by the Society in 2016. He is the only Australian to chair the AP DL Program ever, the only Australian AP DL in almost two decades, and second Australian AP DL ever (after UTS Distinguished Visiting Professor Trevor Bird). He has been continuously serving the IEEE AP Society Administrative Committee in several elected or ex-officio positions since 2015. Karu is also the Chair of the Board of management of Australian Antenna Measurement Facility, and was the elected Chair of both IEEE New South Wales (NSW), and IEEE NSW AP/MTT Chapter, in 2016 and 2017.

Karu has authored approximately 600 research publications and his papers have been cited over 10,000 times. In 2019 his publications received 1,200 citations. He is the first Australian antenna researcher ever to reach Google Scholar h-index of 30 and his citation indices have been among the top Australian antenna researchers for a long time (at present: i10 is 183 and h-index is 49). He is in world's top 100,000 most-cited scientists list by Mendeley Data. Since 2002, his research team has been involved with research grants, contracts and PhD scholarships worth about 20 million dollars, including 15 Australian Research Council grants, without counting the 245 million-dollar SmartSat Corporative Research Centre, which started in 2019. His research has been supported by many national and international organisations including Australian Research Council, Intel, US Air Force, Cisco Systems, Hewlett-Packard, Australian Department of Defence, Australian Department of industry, and German and Indian governments.

Karu's awards include one of the two finalists for 2020 Australian Eureka Prize for Outstanding Mentor of Young Researchers, 2019 Motohisa Kanda Award (from IEEE USA) for the most cited paper in IEEE Transactions on EMC in the past five years, 2019 Macquarie University Research Excellence Award for Innovative Technologies, 2019 ARC Discovery International Award, 2017 Excellence in Research Award from the Faculty of Science and Engineering, 2017 Engineering Excellence Award for Best Innovation, 2017 Highly Commended Research Excellence Award from Macquarie University, 2017 Certificate of Recognition from IEEE Region 10, 2016 and 2012 Engineering Excellence Awards for Best Published Paper from IESL NSW Chapter, 2011 Outstanding Branch Counsellor Award from IEEE headquarters (USA), 2009 Vice Chancellor's Award for Excellence in Higher Degree Research Supervision and 2004 Innovation Award for best invention disclosure. His mentees have been awarded many fellowships, awards and prizes for their research achievements. Fifty-three international experts who examined the theses of his PhD graduates ranked them in the top 5% or 10%. Two of his recent students were awarded PhD with the highest honour at Macquarie University – the Vice Chancellor's Commendation.

Karu has provided expert assistance to more than a dozen companies including Intel, Hewlett Packard Laboratory (USA), Cisco Systems (USA), Audacy (USA), Cochlear, Optus, ResMed and Katherine-Werke (Germany). His team designed the high-gain antenna system for the world's first entirely Ka-band CubeSat made by Audacy, USA and launched to space by SpaceX in December 2018. This is believed to be the first Australian-designed high-gain antenna system launched to space, since CSIRO-designed antennas in Australia's own FedSat launched in 2002.

Karu is in the College of Expert Reviewers of the European Science

Foundation (2019-22) and he has been invited to serve as an international expert/research grant assessor by several other research funding bodies as well, including the European Research Council and funding agencies in Norway, Belgium, the Netherlands, Canada, Finland, Hong-Kong, Georgia, South Africa and Chile. He has been invited by Vice-Chancellors of Australian and overseas universities to assess applications for promotion to professorial levels. He has also been invited to assess grant applications submitted to Australia's most prestigious schemes such as Australian Federation Fellowships and Australian Laureate Fellowships. In addition to the large number of invited conference speeches he has given, he has been an invited plenary/extended/keynote speaker of several IEEE and other conferences and workshops including EuCAP 2020 Copenhagen, Denmark; URSI'19 Seville, Spain; and 23rd ICECOM 2019, Dubrovnik, Croatia.

He is an Associate Editor of IEEE Transactions on Antennas Propagation, IEEE Antennas and Propagation Magazine and IEEE Access. He is a Track Chair pf IEEE AP-S 2020 Montreal, Technical Program Committee Co-Chair of ISAP 2015, APMC 2011 and TENCON 2013 and the Publicity Chair of ICEAA/IEEE APWC 2016, IWAT 2014 and APMC 2000. His research activities are posted in the web at http://web.science.mq.edu.au/esselle/ and https://www.uts.edu.au/staff/karu.esselle .